ADVANCED FUNCTIONAL MATERIALS

Fabrication of Multicomponent Microsystems by Directed Three-Dimensional Self-Assembly**

By *Wei Zheng* and *Heiko O. Jacobs**

We have developed a directed self-assembly process for the fabrication of three-dimensional (3D) microsystems that contain non-identical parts and a statistical model that relates the process yield to the process parameters. The self-assembly process uses geometric-shape recognition to identify different components, and surface tension between liquid solder and metal-coated areas to form mechanical and electrical connections. The concept is used to realize self-packaging microsystems that contain non-identical subunits. To enable the realization of microsystems that contain more than two non-identical subunits, sequential self-assembly is introduced, a process that is similar to the formation of heterodimers, heterotrimers, and higher aggregates found in nature, chemistry, and chemical biology. The self-assembly of three-component assemblies is demonstrated by sequentially adding device segments to the assembly solution including two hundred micrometer-sized light-emitting diodes (LEDs) and complementary metal oxide semiconductor (CMOS) integrated circuits. Six hundred AlGaInP/GaAs LED segments self-assembled onto device carriers in two minutes, without defects, and encapsulation units self-assembled onto the LED-carrier assemblies to form a 3D circuit path to operate the final device. The self-assembly process is a well-defined statistical process. The process follows a first-order, non-linear differential equation. The presented model relates the progression of the self-assembly and yield with the process parameters—component population and capture probability—that are defined by the agitation and the component design.

1. Introduction

The assembly of individual micro- and nanometer-sized devices into integrated systems is a key process of micro- and nanomanufacturing. Traditional manufacturing technologies that focus on assembly include serial pick-and-place, serial wire-bonding, serial packaging, and parallel wafer-to-wafer transfer.[1] As components become smaller, following the trend in miniaturization, conventional robotic methods and assembly lines fail because of the difficulty in building machines that can economically manipulate components in three dimensions that are only micrometers in size. For components with dimensions less than 100 μm, adhesive capillary forces often dominate over gravitational forces, making it difficult to release the components from a robotic manipulator.[2] Micromanipulator-based assembly and wafer-to-wafer transfer methods work poorly on non-planar surfaces, in cavities, and in the fabrication of 3D systems. Serial processes, in general, are slow. Methods of directed self-assembly have the potential to overcome the limitations of robotic assembly and enable the manufacture of multicomponent microsystems in three dimensions.[3–10] Previous demonstrations of directed self-assembly to generate functional electrical microsystems include a fluidic method that positions electronic devices on planar surfaces using shape recognition and gravitational forces;[3,4] liquid-solder-based self-assembly methods that use the surface tension between pairs of molten-solder drops to assemble 3D electrical networks, ring oscillators, and shift registers;[5,6] capillary-force-directed self-assembly that uses hydrophobic–hydrophilic surface patterns and photocurable polymers to integrate micro-optical components, micromirrors, and semiconductor chips on silicon substrates;[7–9] solder–receptor directed self-assembly (where metal contacts on segmented semiconductor devices bind to liquid-solder-based receptors on planar and non-planar surfaces);[10] and capillary-force-driven self-assembly in air to assemble piezoelectric elements of a micropump.[11]

One of the grand challenges in self-assembly is the realization of heterogeneous systems.[12] Although current methods allow the positioning of a large number of identical components in a massively parallel manner, systems that consist of more than one repeating unit are difficult to achieve. In general terms, current procedures provide an insufficient power of recognition to assemble heterogeneous systems correctly. For example, in shape-directed fluidic self-assembly, small device components settle by mistake into the holes designed to match the shape of larger components. Similarly, in surface-tension-driven self-assembly, the binding sites designed for one component will almost always find an overlap with the receptor for a different component. One approach that has been explored to overcome this problem is to activate selected receptors to enable batch transfer of desired components onto desired locations.[13,14]

Herein, we report on recent progress on a different directed self-assembly method[12,15] that could enable the realization of heterogeneous systems that are detached from a common substrate. The systems can be seen as compact aggregates that

[*] Prof. H. O. Jacobs, Dr. W. Zheng
Department of Electrical and Computer Engineering
University of Minnesota
200 Union Street SE, Minneapolis, MN 55455 (USA)
E-mail: hjacobs@ece.umn.edu

[**] This work was supported by the National Science Foundation (grant ECS-0300263).

 © 2005 WILEY-VCH Verlag GmbH & Co. KGaA, Weinheim DOI: 10.1002/adfm.200400595

"grow" in solution. The aggregates form as a result of adding different components to the solution. Our method combines aspects of previous shape-directed fluidic self-assembly[3,4] and solder-based self-assembly methods.[5,6,10] It uses geometric-shape recognition to identify different components, and subsequent bond formation between liquid solder and metal-coated contacts to form mechanical and electrical connections. This combination provides a greater flexibility in the design of self-assembling systems with minimum defects. Another new element is the use of sequential self-assembly.[15] We believe that it will never be possible to assemble complex heterogeneous systems in a single self-assembly step. Instead, we suggest the use of a well-defined sequence. Our idea is borrowed from chemical and biological systems that build heterodimers, trimers, and higher aggregates by sequentially adding different molecules. The concept is similar in the sense that every component type can be seen as a different molecule. In our case, however, each component provides a different functionality. We apply this combination of existing and new concepts to assemble and package microsystems that contain 200 μm sized optoelectronic devices. The components are about 15 times smaller than those used in current robotic assembly lines,[16] 40 times smaller than those of previous solder-based self-assemblies,[5,6] and about the same size as those assembled by shape-directed fluidic procedures on planar surfaces.[3,4] We demonstrate their 3D assembly, registration, and establishment of a 3D circuit path enabling device operation. After a two-step self-assembly sequence, 97 % of encapsulated LEDs displayed the expected function. We report on a statistical model of the self-assembly process. The model relates the assembly time of the self-assembly process and yield with the process parameters: component population and capture probability. The model suggests that self-assembly systems can be realized with many fewer defects than occur in current manufacturing processes. The calculated and experimentally observed assembly time to assemble six hundred LEDs onto device carriers with a yield of 100 % was two minutes.

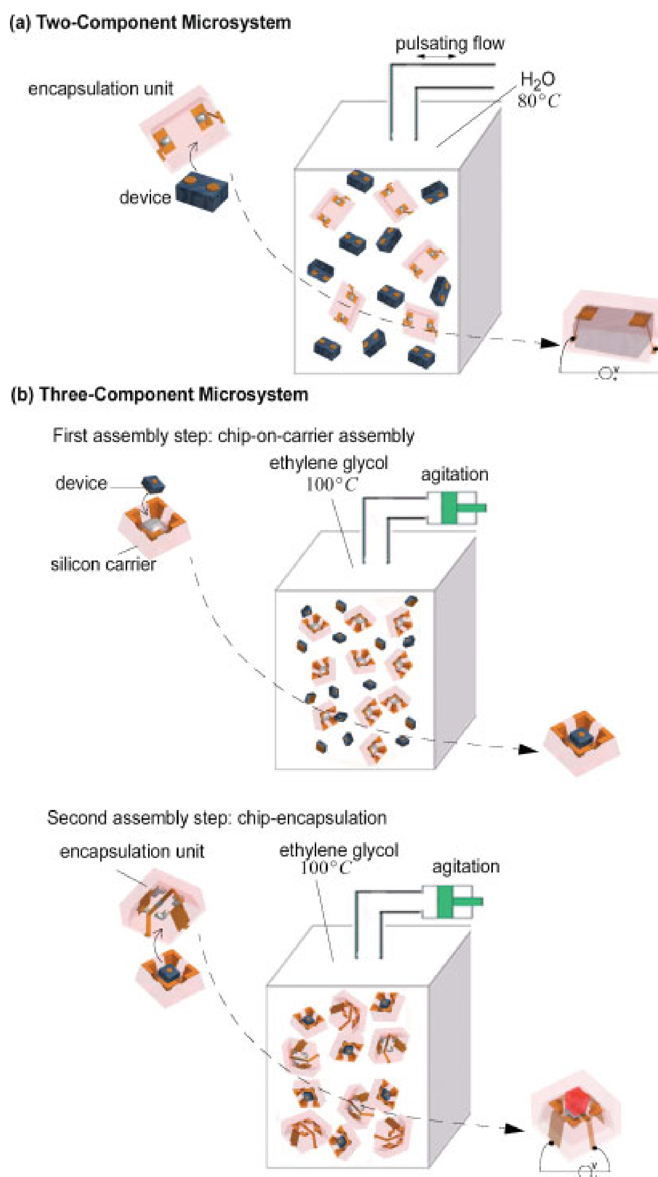

Figure 1. a) Sequential self-assembly and packaging of a two-component microsystem. Self-packaging devices are formed by shape- and surface-tension-directed self-assembly. b) Sequential self-assembly and packaging of a three-component microsystem. The agitated components self-assemble in a two-step sequence and form a 3D circuit path between the device layers. See text for details.

2. Results and Discussion

Figure 1 illustrates the experimental strategy to assemble and package microsystems for two different cases. The first case (Fig. 1a) shows self-packaging chips that are formed by shape- and surface-tension-directed self-assembly in a single sequence. This case is analogous to the formation of heterodimers. The self-packaging devices were formed using two components—a semiconductor-device segment and a Pyrex glass encapsulation unit—with distinct complementary 3D shapes, circuits, solder patterns, and copper metallization. We used LEDs as device segments to construct a system where its function could be tested visually. The LEDs were unpackaged AlGaN/GaN LEDs with a chip size of 380 μm × 330 μm and 80 μm tall (Lginnotek, Korea). The chips have two gold contacts on one side. The components were fabricated using standard micromachining techniques from 500 μm thick Pyrex wafers (Corning 7740, Universitywafer, Boston, MA).[12] To recognize the LEDs during the encapsulation process and to distinguish between encapsulation units themselves, we formed a complementary shaped, 100 μm deep, truncated pyramidal opening in the center of the encapsulation units. Each opening exposed two solder-coated areas to wet and bind to the gold-coated areas on the LED with the complementary shape. During the self-assembly, the surface of the liquid solder wets and binds to the two gold-coated contacts on the front side of the LED segment. The minimization of the free surface area of the liquid solder drives the assembly into a stable aligned position. The solder also provides the electrical connection required to operate the device and the mechanical bond required to hold

 © 2005 WILEY-VCH Verlag GmbH & Co. KGaA, Weinheim

the assembly together. We used a low-melting alloy (Y-LMA-117, melting point mp ≈ 47 °C, Small Parts, Miami Lakes, FL) of bismuth, lead, tin, cadmium, and indium as the solder. This solder has been used in a previous self-assembly experiment[10,17] because it has a high surface energy (≈ 400 mJ m^{-2}).

The second case (Fig. 1b) shows the sequential assembly and packaging of three-component microsystems. This case is analogous to the formation of heterodimers. Each microsystem consists of three parts—a semiconductor device segment, a silicon carrier, and a Pyrex encapsulation unit—with distinct complementary 3D shapes, circuits, solder patterns, and copper metallization. The assembly is formed by a two-step sequence of self-assembly and packaging: i) chip-on-carrier assembly, and ii) chip encapsulation. The device segments were unpackaged cubic AlGaInP/GaAs LED segments with side lengths of 200 μm (TK508DR, Tyntek, Taiwan). The chips have two contacts: a small circular anode on the front, and a large square cathode covering the back. The assembly process of each step is similar to the first case described above. The procedure to fabricate the silicon carriers, Pyrex encapsulation units, circuits, and patterned solder drops on the 3D-shaped units is shown in Figure 2 and described in Section 4.

We used water as the self-assembly solution in the first case (Fig. 1a) and ethylene glycol in the second case (Fig. 1b). The water and ethylene glycol solutions were made slightly acidic (pH 2.5) with sulfuric acid to remove metal oxides from the surface of the solder and copper-binding sites. An important limitation of water is its low boiling point, which prohibits the use of high-melting point solders. To overcome this limitation, a number of alternatives to water as the self-assembly solvent were considered. The solvent needs to have a high boiling point, and must not react with the solder, copper, glass, silicon, or the photoresist. It must dissolve the acid required to remove surface oxides from solder pads and copper contacts, and should not react with this acid. To avoid contamination of the solder and copper surfaces with salts, this solvent must also dissolve the metal salts that form by the reaction of the acid with the metal oxides and the metals. The self-assembly solvent should wet the components to prevent the formation of trapped air bubbles in recesses, such as the tapered opening in the device carriers, because air bubbles interfere with the self-assembly process. It appears that ethylene glycol and several of its derivatives may fulfill these requirements. Long-chain hydrocarbons including dodecane and hexatriacontane are also good candidates. In order to prove the feasibility of solder-based self-assembly in high-boiling-point solutions, we used a high-melting-point solder (LMA-281, mp ≈ 138 °C, Small Parts, Miami Lakes, FL) to perform self-assembly experiments in both ethylene glycol (boiling point 197 °C) at 150 °C and tetraethylene glycol (boiling point 328 °C) at 200 °C. We did not observe a notable difference between the quality of the self-assembled structures formed in water, ethylene glycol, or tetraethylene glycol.

We built a turbulent pulsating-flow system to provide a strong and reproducible form of agitation. We also tested agitation of the components by shaking the vial manually; however, the results were less reproducible. The turbulent pulsating flow was created using a piston pump (PM6014, Fluid Metering, Inc., Syosset, NY) that expels and retracts liquid through a 2 mm diameter nozzle that is submerged in the assembly solution. The amount and frequency of liquid that is cycled back and forth can be adjusted between 1 and 1.5 mL, and 0 and 10 Hz, respectively. The assembly was carried out inside a rectangular glass container (12 mm on each side and 45 mm high) filled with 4.5 mL of assembly solution. The energy gain due to the surface tension S scales with the area x^2 of the involved interfaces and is given as $E_s = Sx^2$.[18] The disordering energy due to the pulsating flow shows a similar x^2 relationship if we consider spherical components with a diameter x and a pulsating laminar flow of velocity v. The energy change due to flow as a function of the displacement x can then be calculated by integrating Stokes' law and becomes $E_d = 3\pi\eta v x^2$, where η is the dynamic viscosity of the liquid. Turbulent flow has a number of advantages compared with tumbling or external acceleration.[12] Good mixing of components with different densities can be accomplished while maintaining an adjustable balance between the disordering and ordering energies for components with different dimensions. The disordering energy due to the drag in a liquid flow and the ordering energy due to surface tension between components can be adjusted to have similar magnitudes. This may be beneficial in self-assemblies where the level of agitation needs to be adjusted to overcome local energy minima in the space of possible conformations.

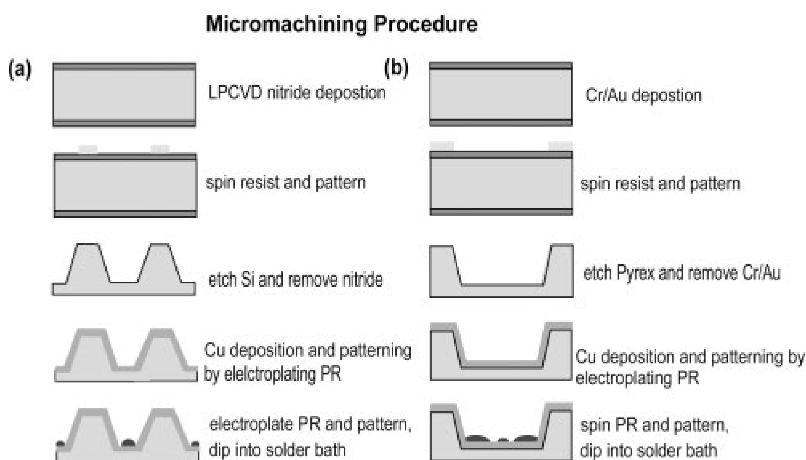

Figure 2. Micromachining procedure illustrating the processing steps to fabricate a) the silicon carriers and b) the Pyrex encapsulation units. The process details are described in the experimental section. Abbreviations: LPCVD, low-pressure chemical vapor deposition; PR, photoresist.

The experimental realization of the different microsystems is illustrated in Figure 3. The first case (Fig. 3a) shows the assembly process of self-packaging chips formed using two components in a single sequence. We added 1000 AlGaN/GaN blue LED chips and 200 encapsulation units into the heated assembly solution and agitated the

 © 2005 WILEY-VCH Verlag GmbH & Co. KGaA, Weinheim

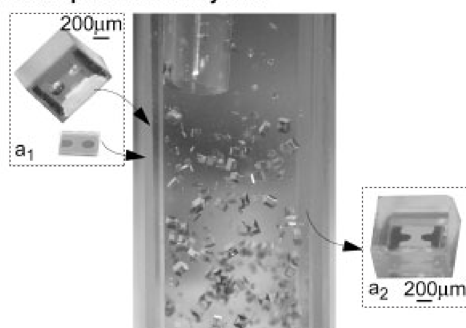

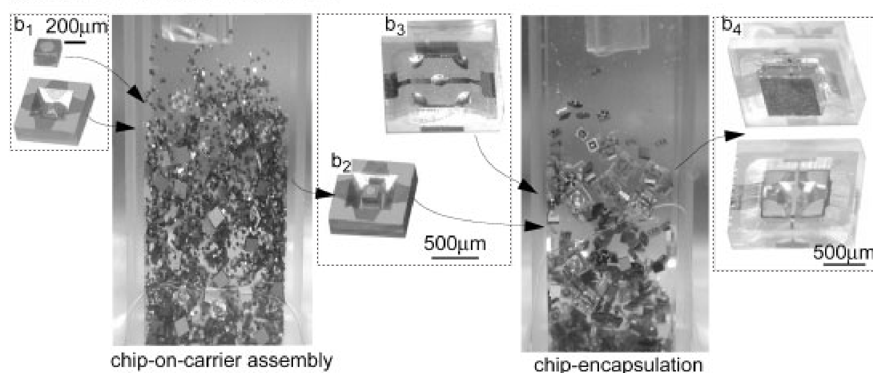

Figure 3. a) Photograph of two-component self-packaging LEDs where close-ups show the device components before (inset a_1) and after (inset a_2) assembly. b) Photographs of three-component microsystem assembly and packaging using a two-step chip-on-carrier assembly and chip-encapsulation sequence. Close-ups (insets b_1–b_4) show the device components before and after each assembly step.

on the front side. The procedure and yield to assemble and package these devices were similar to those described for the blue LED segments.

Our self-assembly process is a stochastic assembly process. Previously reported stochastic models of self-assembly include a model of DNA self-assembly to optimize time and program size based on the Markov process,[19] a stochastic model of a self-assembled nanowire address decoder,[20] and an analytical model of stochastic self-reconfigurable cellular robotics.[21] None of the above models have produced a mathematical relationship between the assembly environment and assembly rate and yield. We believe that mathematical models that describe the formation of heterodimers and heterotrimers as a function of molar concentrations would be the most appropriate starting point. However, we have not yet found an appropriate model that describes our process. The following outlines a first-order model of our process in order to better understand our experimental observations. Experimentally, we observed that the progression of the self-assembly was nonlinear: the rate of self-assembly of the LEDs on the carriers was faster in the beginning and slowed down with the reduction of available LEDs and unoccupied carriers in the assembly volume. An increase in the number of excess LEDs increased the speed and yield of the process. To obtain a mathematical model of the assembly process, we considered a fixed volume that contained c carriers and l LEDs. We assumed that the mixing, capture probabilities, and capture rates between individual compo-

pieces. The self-assembly process reached a steady state in three minutes. The second case (Fig. 3b) shows the sequential assembly and packaging of three-component microsystems. For the chip-on-carrier assembly, 3000 AlGaInP/GaAs red LED chips and 600 carrier units were added into the heated assembly solution. Each silicon carrier provided a binding site—a 200 µm wide square-shaped solder-coated area—in the center of the 200 µm deep, tapered opening to bind to the gold-coated cathode on the back side of the LEDs during the self-assembly step. We obtained a yield of 100 %; that is, all 600 carriers captured an LED device segment in two minutes. For the chip-encapsulation, we removed the excess LEDs by filtration through a 500 µm mesh filter and added 200 encapsulation units to the assembly container. The excess LEDs were reused in later experiments. Each encapsulation unit exposed five solder-coated areas in the center of a 200 µm deep, tapered opening to wet and bind to gold-coated areas with complementary shapes on the LED and carrier during the encapsulation process. We tested the functionality by surface mounting the two types of devices by hand on a printed circuit board (Fig. 4); 95 % of the blue LEDs and 97 % of the red LEDs functioned after applying an external voltage. Besides the LED segments, we successfully assembled three-terminal silicon integrated circuits carrying metal oxide semiconductor (MOS) transistors. The silicon segments with integrated MOS transistors had three contacts

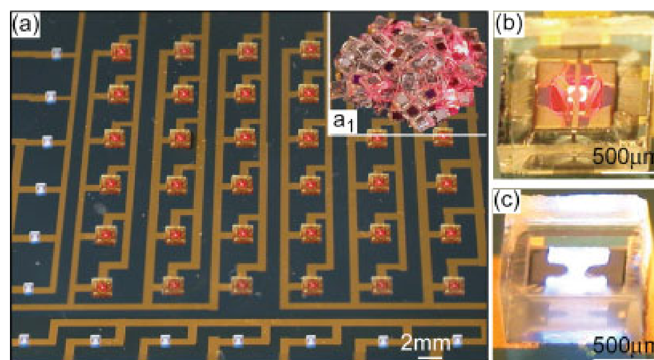

Figure 4. Testing of LED chips that were assembled and packaged by directed 3D self-assembly. a) Test of an array of red and blue LEDs that were hand-mounted on a printed circuit board. The inset (a_1) shows a photograph of a cluster of 200 encapsulated devices that were assembled in 4 min. b,c) Close-up photographs of the red (b) and blue (c) LED assemblies in the ON state that visualize the formation of 3D circuit paths between the different device layers and the printed circuit board.

 © 2005 WILEY-VCH Verlag GmbH & Co. KGaA, Weinheim

nents are time-invariant and independent of the component population. This assumption will be incorrect in cases where the components reach too high a population, such that mixing and component transport become impaired. In our situation, the components occupied less than 20 % of the assembly volume.

Under these assumptions, we can define a probability $P_{i,n}$ that LED L_i is captured by the receptor C_n within a time interval of τ. The capture probability $P_{i,n}$ is time-invariant and independent of the indices i and n, and is only a function of the receptor design, component shape, volume, mixing speed, and length of the experiment. $P_{i,n}$ would also be equal to the probability of capture in an experiment where there is only one single LED and one single receptor within the volume. $P_{i,n}$ would increase with the time interval τ of the experiment and can be written as

$$P_{i,n} = (\partial P/\partial t)\tau = p\tau = (1/T)\tau \tag{1}$$

where p and T denote an average capture rate and time, respectively, and can be determined experimentally: they are the average capture rate and time that are observed if the volume contains a single LED and a single carrier.

The characteristic "single-component–single-carrier" capture time and rate are the most important process parameters. They are defined by the layout of the solder pattern, binding sites, component shape, volume, and mixing speed. The single-component–single-carrier capture time and rate define the overall time, rate, and yield of any process with c identical carriers and l identical LEDs. For example, the probability of an unoccupied carrier C_n capturing an LED out of a pool of l available LEDs is l times as large in the beginning of the assembly process and reduces to $(l–a)P_{i,n}$ after a assembly events. Similarly, the average capture rate $a' = \partial a(t)/\partial t$ reduces to $a' = (l–a)/T$ for a single carrier and $a' = (c–a)(l–a)/T$ for $c–a$ carriers that remain unoccupied after a assembly events. The last equation describes our self-assembly process: it is a nonlinear, first-order differential equation that combines the assembly rate $a' = \partial a(t)/\partial t$ with the number of self-assembly events $a(t)$ that took place. As a solution, we obtain

$$a(t) = c(e^{(l-c)t/T} - 1)/(e^{(l-c)t/T} - c/l) \tag{2}$$

which describes the progression of the self-assembly as a function of time. Equation 2 illustrates that the progression of the self-assembly is only a function of three parameters: the component population l, c, and the single-component–single-carrier capture time T; it describes the progression of the self-assembly process as a function of time. Progression in the context presented here means the sum of assembled components as a function of time. We note that the progression of the assembly process is a discrete process; that is, the sum of the self-assembly events is an integer, not a continuous function. However, we used a continuous formalism to control the complexity of the equations. A discrete formalism that makes use of discrete series should yield the same result. We tried this approach but the equations became exceedingly complex.

Figure 5 compares the calculated progression of the self-assembly with three experiments varying the component population by increasing the number of available excess LEDs. In each experiment we used 100 carriers, an assembly volume of 4.5 mL, and an intermediate level of agitation (1.0 mL, 3 Hz).

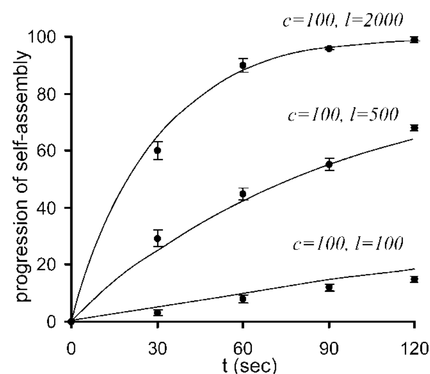

Figure 5. Calculated and measured progression of the self-assembly onto 100 carriers in the presence of 100, 500, and 2000 LEDs. Error bars show the standard deviations of three data sets. The solid curves represent the calculated values from Equation 2 with $T = 15$ h.

The experiments were interrupted after 30, 60, 90, and 120 s to count the carriers that captured an LED. In the first experiments, we used an equal number (100) of LEDs and carriers, so that Equation 2 reduced to

$$a(t) \underset{l \to c}{=} c/(1 + T/(tc)) \tag{3}$$

and we observed a constant assembly rate and a linear progression in the recorded time interval. Outside the illustrated time interval, we expect an asymptotic limit. In the second and third experiments, we increased the number of available LEDs to 500 and 2000, respectively, and observed an increased progression in the self-assembly that slowed down as the yield approached the asymptotic limit of 100 %. In all three cases, we found good agreement between the experimental data and our model for an average single-component–single-carrier capture time T of 15 h. With 2000 LEDs in the assembly solution, all carriers captured a device within two minutes. We also noticed that the yield of the self-assembly process increased exponentially with the assembly time. The yield is the ratio of the number of assembled device segments a to the total number of carriers c. Equation 2 can be used to calculate the assembly time $t = T/(l–c)[\ln(1–a/l)–\ln(1–a/c)]$ to get a desired yield a/c. The first $\ln(1–a/l)$ part of this equation is a negative number that can be neglected if the number of available LEDs is large compared to the number of carriers. The equation for the required assembly time becomes $t = T/(l–c)[–\ln(1–a/c)]$ in this case, and $(2.3\,T)/(l–c) \times 2$, $(2.3\,T)/(l–c) \times 3$, and $(2.3\,T)/(l–c) \times 4$ for yields of 99 %, 99.9 %, and 99.99 %, respectively. These equations reflect the parallel nature of the self-assembly process and suggest that a larger number of carriers could be assembled in the same time with similar yields. The calculated assembly times

 © 2005 WILEY-VCH Verlag GmbH & Co. KGaA, Weinheim

for obtaining the desired yield are mainly a function of the number of excess LEDs (l–c) and the process parameter T, and not a function of the number of carriers. The results indicate an exponential improvement in the yield is possible with a linear increase in the assembly time. This corrects a common misperception that statistical self-assembly cannot achieve yields that are similar to deterministic assembly.

The presented theory is a first-order estimate. Ultimately, there are a maximum number of components that can be suspended in a given volume, and high component densities will affect the self-assembly process. Component impaction, for example, can result in component damage, and imperfections in the manufacturing process of the components can reduce the asymptotic limit. The transport of components would become impaired at high component populations and reduce the speed of the assembly process. We have not established the component density that is required to enter a transport-limited regime. We conclude that many defects that are present in our and other self-assembly systems are not related to the self-assembly process, but to the imperfections in the manufacturing of the components and the imperfect designs of the self-assembly systems.

Directed 3D self-assembly, when compared with existing self-assembly techniques,[3–10] excludes a number of defects that are frequently an integral part of self-assembly processes. Defects integral to self-assembly processes are most commonly related to local energy minima in the space of possible conformations, or to an insufficient overall energy minimum to form a stable assembly under agitation. We were able to remove energy-minima-related defects completely by introducing and optimizing complementary shapes and by using a well-defined sequence. The first carrier designs, for example, had a large opening and captured two device segments at a time—a defect that was removed by reducing the size of the opening. We also observed the detachment of the assembled components as a result of component impaction. We removed this defect by integrating the semiconductor device segments in a protected, recessed region, and by increasing the binding sites on the carriers to cover at least 40 % of the surface. We found no defects that are integral to the self-assembly itself and that intrinsically limit the level of perfection that can be achieved.

3. Conclusions

We have demonstrated the self-assembly and packaging of microsystems using a directed 3D self-assembly technique that combines existing concepts—geometric-shape recognition and site-specific wetting and binding involving liquid solder—with a new concept of sequential self-assembly. The technique is tailored to enable the realization of heterogeneous, 3D microsystems containing non-identical parts and to connect them electrically. The shape provides the ability to recognize different components, where the solder provides both the driving force and the electrical and mechanical connections, and the sequence provides the ability to build complex systems.

We believe the three-fold combination provides, for the first time, a route to the realization of complex systems. The design capability of "single energy minimum" systems is greatly enhanced; many solutions become available to solve a given design problem. The concept could find application in the microelectromechanical system (MEMS) community and in the realization of systems that contain sensors, actuators, or microfluidic elements. Self-assembly-based manufacturing is a new field that has a lot to offer compared with traditional robotic assembly lines: high-throughput assembly, 3D topologies, and the ability to handle smaller components are the most important advantages. A potential disadvantage of self-assembly is that it requires components that can effectively direct the self-assembly process. This additional effort can be limited if conventional surface micromachining is used. The use of unconventional methods, where the components can be patterned on all faces, however, would provide even greater flexibility in the creation of 3D systems.

4. Experimental

Fabrication of Silicon Carriers: A p-type 280 μm thick silicon wafer (Virginia Semiconductor, Fredericksburg, VA) was coated with nitride by low-pressure chemical vapor deposition (LPCVD) to form a 100 nm thick layer. The substrate was primed with hexamethyldisilazane and spin-coated with photoresist (Microposit 1813, Shipley, Phoenix, AZ). After a soft-bake at 105 °C for 1 min, the substrate was exposed to UV light through a dark-field mask. The photoresist was developed in MIF-351/H_2O (1:5 v/v) developer for about 15 s. The exposed nitride area was etched in a STS etcher for 2 min; the exposed silicon area was etched in KOH (45 %) at 80 °C for 4.5 h, resulting in a 200 μm deep tapered opening. After etching, the silicon wafer was coated with 25 nm titanium and 800 nm copper using an e-beam evaporator. Shipley Eagle 2100 photoresist was electroplated on the wafer using a direct-current (DC) voltage (50 V) for 30 s at 35 °C. After a soft-bake at 80 °C for 2 min, the substrate was exposed to UV light through the second mask for 60 s. The Eagle 2100 photoresist was developed in Eagle 2005 developer/H_2O (1:24 v/v), at 38 °C for 2 min. The exposed copper was etched in an aqueous ferric chloride solution (1.4 g of $FeCl_3$ per milliliter of H_2O, pH 1.3) and the titanium was etched in 10:1 buffered oxide etchant. After removing the Eagle 2100 photoresist in acetone, another layer of Eagle 2100 photoresist was electroplated using a DC voltage (50 V) for 30 s at 35 °C to form the solder-coated receptors. The photoresist was exposed and developed using the same conditions as described before. The exposed copper squares were coated with solder (Y-LMA-117, melting point mp ≈ 45 °C, Small Parts, Miami Lakes, FL) by immersing the substrate in a solder bath. Finally, the wafer was diced using an automated dicing saw to obtain the silicon carriers. The remaining photoresist was removed in acetone to expose the binding sites.

Fabrication of Pyrex Encapsulation Units: A 500 μm thick Corning 7740 wafer (Universitywafer, Boston, MA) was coated with 25 nm chromium and 250 nm gold using an e-beam evaporator. The substrate was primed with hexamethyldisilazane and spin-coated with photoresist (Microposit 1813, Shipley, Phoenix, AZ). After a soft-bake at 105 °C for 1 min, the substrate was exposed to UV light through a dark-field mask. The photoresist was developed in MIF-351/H_2O (1:5 v/v) developer for about 15 s. The metal layers were etched using $KI/I_2/H_2O$ (4:1:40 v/v/v) for gold and HCl/glycerol/H_2O (1:1:3 v/v/v) for chromium. The exposed glass area was etched in HF (49 %)/NHO_3 (69 %)/H_2O (20:14:66 v/v/v) for 5 h. After removing the metal layer, the glass wafer was coated with 25 nm titanium and 800 nm copper using an e-beam evaporator. The Shipley Eagle 2100 photoresist was electroplated on the wafer using a DC voltage (50 V) for 30 s at 35 °C. After a soft-bake at 80 °C for 2 min, the substrate was exposed to UV light through the second mask for 60 s. The Eagle 2100 photoresist was

© 2005 WILEY-VCH Verlag GmbH & Co. KGaA, Weinheim

developed in Eagle 2005 developer/H_2O (1:24 v/v) at 38 °C for 2 min. The exposed copper was etched in an aqueous ferric chloride solution (1.4 g of $FeCl_3$ per milliliter of H_2O, pH 1.3) and the titanium was etched in 10:1 buffered oxide etchant. After removing the Eagle 2100 photoresist in acetone, the Shipley 1805 photoresist was spun on the substrate and patterned to expose the copper area for solder wetting. The opening area was coated with the low-melting-point solder (Y-LMA-117, mp ≈ 45 °C, Small Parts, Miami Lakes, FL) by immersing the substrate in a solder bath. Finally, the wafer was diced to obtain the Pyrex encapsulation units. The remaining photoresist was removed in acetone to expose the binding sites.

Control of Surface Chemistries: The surfaces must be free from organic contaminants and oxides for the self-assembly process to work. We cleaned the LEDs, silicon carriers, and Pyrex encapsulation units in acetone, methanol, and concentrated sulfuric acid before transferring them into the water and ethylene glycol solution. We added a small amount of sulfuric acid (approximately pH 2.5) to dissolve oxides (formed from residual oxygen) in the water and ethylene glycol. It was necessary to adjust the pH carefully to avoid dissolution of the solder itself.

Received: December 18, 2004
Final version: January 27, 2005

[1] M. B. Cohn, K. F. Bohringer, J. M. Noworolski, A. Singh, C. G. Keller, K. Y. Goldberg, R. T. Howe, *Proc. SPIE—Int. Soc. Opt. Eng.* **1998**, *3512*, 2.
[2] R. S. Fearing, presented at the Int. Conf. on Intelligent Robots and Systems (IROS 1995), Pittsburgh, PA, August 1995.
[3] H. J. Yeh, J. S. Smith, *IEEE Photonics Technol. Lett.* **1994**, *6*, 706.
[4] J. S. Smith, H. J. Yeh, *US Patent 5 824 186*, **1998**.
[5] D. H. Gracias, J. Tien, T. L. Breen, C. Hsu, G. M. Whitesides, *Science* **2000**, *289*, 1170.
[6] M. Boncheva, D. H. Gracias, H. O. Jacobs, G. M. Whitesides, *Proc. Natl. Acad. Sci. USA* **2002**, *99*, 4937.
[7] U. Srinivasan, D. Liepmann, R. T. Howe, *J. Microelectromech. Syst.* **2001**, *10*, 17.
[8] U. Srinivasan, M. A. Helmbrecht, C. Rembe, R. S. Muller, R. T. Howe, *IEEE J. Sel. Top. Quantum Electron.* **2002**, *8*, 4.
[9] K. F. Böhringer, U. Srinivasan, R. T. Howe, presented at Int. Conf. on Micro Electro Mechanical Systems (MEMS 2001), Interlaken, Switzerland, January 2001.
[10] H. O. Jacobs, A. R. Tao, A. Schwartz, D. H. Gracias, G. M. Whitesides, *Science* **2002**, *296*, 323.
[11] J. Fang, K. Wang, K. F. Böhringer, presented at Int. Conf. on Solid State Sensor, Actuator, and Microsystems Workshop, Hilton Head Island, SC, June 2004.
[12] W. Zheng, H. O. Jacobs, *Appl. Phys. Lett.* **2004**, *85*, 3635.
[13] X. Xiong, Y. Hanein, J. Fang, Y. Wang, W. Wang, D. T. Schwartz, K. F. Bohringer, *J. Microelectromech. Syst.* **2003**, *12*, 117.
[14] C. R. Barry, C. J. Hoon, H. O. Jacobs, presented at Int. Conf. on Foundations of NanoScience: Self-Assembled Architectures and Devices, Snowbird, UT, April 2004.
[15] W. Zheng, P. Buhlmann, H. O. Jacobs, *Proc. Natl. Acad. Sci. USA* **2004**, *101*, 12 814.
[16] M. Walz, *Circuits Assem.* **2003**, *1*, 32.
[17] T. L. Breen, J. Tien, S. R. J. Oliver, T. Hadzic, G. M. Whitesides, *Science* **1999**, *284*, 948.
[18] K. S. Birdi, *Self-assembly Monolayer Structures of Lipids and Macromolecules at Interfaces*, Kluwer, New York **1999**.
[19] L. Adleman, Q. Cheng, A. Goel, M. Huang, presented at ACM Symp. on Theory of Computing, Hersonissos, Greece, July 2001.
[20] A. DeHon, P. Lincoln, J. E. Savage, *IEEE Trans. Nanotechnol.* **2003**, *2*, 165.
[21] P. J. White, K. Kopanski, H. Lipson, presented at Int. Conf. on Robotics and Automation (ICRA 2004), New Orleans, LA, April 2004.

 © 2005 WILEY-VCH Verlag GmbH & Co. KGaA, Weinheim